Comput Geosci (2017) 21:921–936
DOI 10.1007/s10596-017-9669-5

ORIGINAL PAPER

Higher resolution total velocity *Vt* and *Va* finite-volume formulations on cell-centred structured and unstructured grids

Ya-wei Xie[1] · **Michael G. Edwards**[1]

Received: 15 October 2016 / Accepted: 1 June 2017 / Published online: 5 September 2017

Abstract Novel cell-centred finite-volume formulations are presented for incompressible and immiscible two-phase flow with both gravity and capillary pressure effects on structured and unstructured grids. The Darcy-flux is approximated by a control-volume distributed multipoint flux approximation (CVD-MPFA) coupled with a higher resolution approximation for convective transport. The CVD-MPFA method is used for Darcy-flux approximation involving pressure, gravity, and capillary pressure flux operators. Two IMPES formulations for coupling the pressure equation with fluid transport are presented. The first is based on the classical total velocity *Vt* fractional flow (Buckley Leverett) formulation, and the second is based on a more recent *Va* formulation. The CVD-MPFA method is employed for both *Vt* and *Va* formulations. The advantages of both coupled formulations are contrasted. The methods are tested on a range of structured and unstructured quadrilateral and triangular grids. The tests show that the resulting methods are found to be comparable for a number of classical cases, including channel flow problems. However, when gravity is present, flow regimes are identified where the *Va* formulation becomes locally unstable, in contrast to the total velocity formulation. The test cases also show the advantages of the higher resolution method compared to standard first-order single-point upstream weighting.

✉ Ya-wei Xie
717023@swansea.ac.uk

Michael G. Edwards
m.g.edwards@swansea.ac.uk

[1] Zienkiewicz Centre for Computational Engineering, College of Engineering, Swansea University, Swansea, SA1 8EN, UK

Keywords Cell-centred finite-volume · Higher resolution method · Two-phase flow · Gravity · Capillary pressure · *Vt* and *Va* formulations · CVD · MPFA

1 Introduction

Novel cell-centred finite-volume Implicit Pressure-Explicit Saturation (IMPES) formulations are presented for the solution of incompressible, immiscible two-phase flow problems involving gravity and capillary pressure on structured and unstructured grids. The Darcy-flux is approximated by a control-volume distributed multipoint flux approximation (CVD-MPFA) [6] coupled with a higher resolution approximation for convective transport [1, 5]. The symmetric CVD-MPFA method is used for Darcy-flux approximation including pressure, gravity, and capillary pressure flux components.

The IMPES method is one of the key solution strategies for solving coupled systems of multi-phase flow equations in petroleum reservoir simulation, e.g., [13], and has the advantage of reducing the size of the linear systems to be solved, compared to a fully implicit (FI) method. However, we note that by definition, sequential methods cannot satisfy all of the flow equations exactly at each time step of the computation, further discussion is given in [2]. Two formulations for coupling the pressure equation with fluid transport are presented. The first is based on the classical total velocity *Vt* fractional flow (Buckley Leverett) formulation and the second is based on a more recent *Va* formulation, proposed by Karimi-Fard and Firoozabadi [4] and used in [8, 9, 15]. The CVD-MPFA method is employed here for both *Vt* and *Va* formulations. A well-known fundamental point in favour of the total velocity formulation is that *Vt* is spatially constant in one dimension and slowly varying

in higher dimensions, making this a natural candidate for IMPES splitting [2]. The *Vt* formulation also enables formal identification of the respective hyperbolic, parabolic and elliptic character types of the flow equations that are routinely embedded in the coupled system, and consequently aids optimal design in approximation of the resulting fluxes. The saturation equation can be solved numerically by Godunov's finite-volume method [11]. Brenier and Jaffre [16] compared several numerical schemes for flow with gravity, including Godunov's method, and an explicit version of the upstream mobility (UM) scheme is introduced. It is shown that the viscosity of the UM scheme is greater than that of the Godunov method. In [17], Kaasschieter used the Godunov method to solve BL equation with gravity, and analysed the entropy conditions for solution uniqueness. Local Lax Friedrichs (LLF)-based methods for two-phase and three component two-phase flow with gravity segregation are presented in [7], using both global and local central non-upwind schemes for a range of gravity numbers. In the work presented here, capillary pressure is considered together with gravity and convective forces and coupled via a time splitting formulation that enables the time-step size to only be governed by the convective CFL condition, while capillary pressure terms are computed implicitly.

In this paper, the advantages of both coupled formulations are contrasted. The methods are tested on a range of structured and unstructured quadrilateral and triangular grids. The tests show that the resulting methods are found to be comparable for a number of classical cases, including quarter five spot and channel flow problems. However, when gravity is present, flow regimes are identified where the *Va* method becomes locally unstable, in contrast to the total velocity formulation. The test cases also show the advantages of the higher resolution method compared to standard first order single point upstream weighting.

2 Incompressible and immiscible two-phase flow

Incompressible and immiscible two-phase flow is considered in this paper with water as wetting phase and oil as non-wetting phase. Following [13] the phase velocities are given by Darcy's law:

$$\vec{v}_o = -\mathbf{K}\frac{k_{ro}}{\mu_o}(\nabla p_o - \rho_o g \nabla h) \tag{1}$$

$$\vec{v}_w = -\mathbf{K}\frac{k_{rw}}{\mu_w}(\nabla p_w - \rho_w g \nabla h) \tag{2}$$

together with the continuity equation for each phase:

$$\Phi\frac{\partial s_o}{\partial t} + \nabla\cdot\vec{v}_o = q_o \tag{3}$$

$$\Phi\frac{\partial s_w}{\partial t} + \nabla\cdot\vec{v}_w = q_w \tag{4}$$

where the convention here for the positive of the z-coordinate, i.e., h, is in the vertical downward direction along the z-axis. The subscripts o and w represent the non-aqueous and aqueous phases respectively. The phase saturations satisfy the volume balance

$$s_w + s_o = 1. \tag{5}$$

Capillary pressure is the difference between the oleic and aqueous phase pressures:

$$p_c = p_o - p_w. \tag{6}$$

The *Vt* and *Va* formulations of the governing equations (1)–(6) are presented below.

2.1 Governing equations: *Vt* formulation

The governing equations are written in the *Vt* fractional flow form with:
The pressure equation

$$\nabla\cdot\vec{v}_T = q \tag{7}$$

and the water phase saturation equation

$$\Phi\frac{\partial s}{\partial t} + \nabla\cdot\vec{v}_w = q_w \tag{8}$$

where

$$\vec{v}_w = f_w(\vec{v}_T + \lambda_o\Delta\rho g\mathbf{K}\nabla h + \lambda_o\mathbf{K}\nabla p_c), \tag{9}$$

and the total velocity $\vec{v}_T$ is defined by

$$\vec{v}_T = -\lambda_T\mathbf{K}\nabla p + (\lambda_w\rho_w + \lambda_o\rho_o)g\mathbf{K}\nabla h + \lambda_w\mathbf{K}\nabla p_c. \tag{10}$$

Here, $p = p_o$ is the oleic pressure, $s = s_w$ is the aqueous phase saturation, $f_w(s) = \lambda_w/\lambda_T$ is the fractional flow involving the ratio of aqueous phase mobility λ_w to total mobility $\lambda_T = \lambda_w + \lambda_o$, $\lambda_o = \frac{k_{ro}}{\mu_o}$, $\lambda_w = \frac{k_{rw}}{\mu_w}$, and $\mathbf{K}$, ∇p_c, Φ, q_w are the absolute permeability, capillary pressure gradient, porosity and aqueous source term respectively. The definition of the total source term is given by $q = q_o + q_w$, the density difference is $\Delta\rho = \rho_w - \rho_o$, and oil saturation s_o is deduced from (5).

2.2 Governing equations: *Va* formulation

The governing equations are now written in the *Va* "fractional flow" form with:
The pressure equation

$$-\nabla\cdot(\lambda_T\mathbf{K}\nabla\Psi_w + \lambda_o\mathbf{K}\nabla\Psi_c) = q \tag{11}$$

and the water phase continuity equation

$$\Phi\frac{\partial s}{\partial t} + \nabla\cdot(f_w\vec{v}_a) = q_w, \tag{12}$$

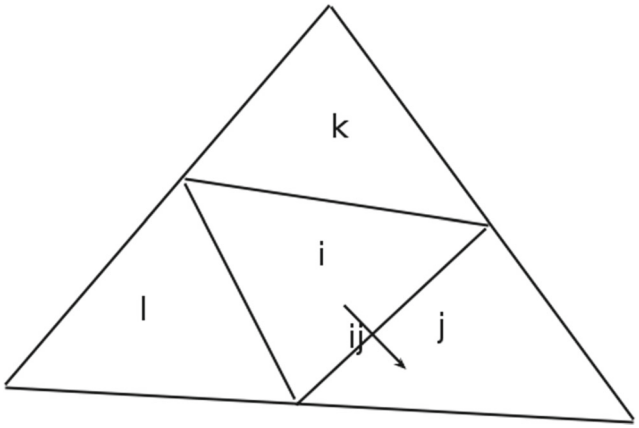

Fig. 1 stencils for reconstrcution and limiting in unstructured mesh

where

$$\Psi_i = p_i - \rho_i g h, i = w, o, \tag{13}$$

$$\vec{v}_a = -\lambda_T \mathbf{K} \nabla \Psi_w, \tag{14}$$

with the flow potential variable defined as

$$\Psi_c = p_c + \Delta \rho g h, \tag{15}$$

which was first introduced in [4]. Here, λ_T, $\mathbf{K}$, p, Φ and q are the total mobility, absolute permeability, non-aqueous pressure, porosity and total source term, s and $f_w = \lambda_w / \lambda_T$ are the aqueous saturation and fractional flow.

The *Va* formulation has some clear advantages when treating capillary pressure, e.g., Hoteit and Firoozabadi [9], Friis et al. [8], Bastian [15]: Apart from convective terms, the need for nonlinear (Newton) iteration is eliminated due to the explicit treatment of capillary pressure in the *Va* formulation, which is an advantage computationally and from the implementation point of view. The *Va* formulation also facilitates a much more straightforward CVD-MPFA implementation of the capillary pressure operator. This task is more challenging for the standard *Vt* formulation which also includes a non-linear capillary pressure diffusion operator which has to be approximated via a CVD-MPFA operator, and requires implicit nonlinear iteration to overcome the explicit diffusivity time step limit. The *Va* formulation involves upwinding the saturation flux of Eq. 12 according to the sign of the *Va* wave speed, and when gravity is considered an upwind mobility approximation is used for the second term in the pressure Eq. 11, to ensure stability. The *Va* formulation time step is dependent on a CFL condition based on $\vec{v}_a$, whereas the *Vt* formulation time step depends on the actual wave speed. We also note that in contrast, the standard approach involves upwinding on phase velocities, Aziz and Settari [13], further methods are also proposed, e.g., Wheeler et al. [18].

2.3 The IMPES method

Further details of the IMPES method can be found in e.g. [12] and [13]. Here, we discuss aspects of the *Vt* and *Va* formulations. The pressure and saturation equations are formulated as shown in the respective sections 2.1 and 2.2 above, and

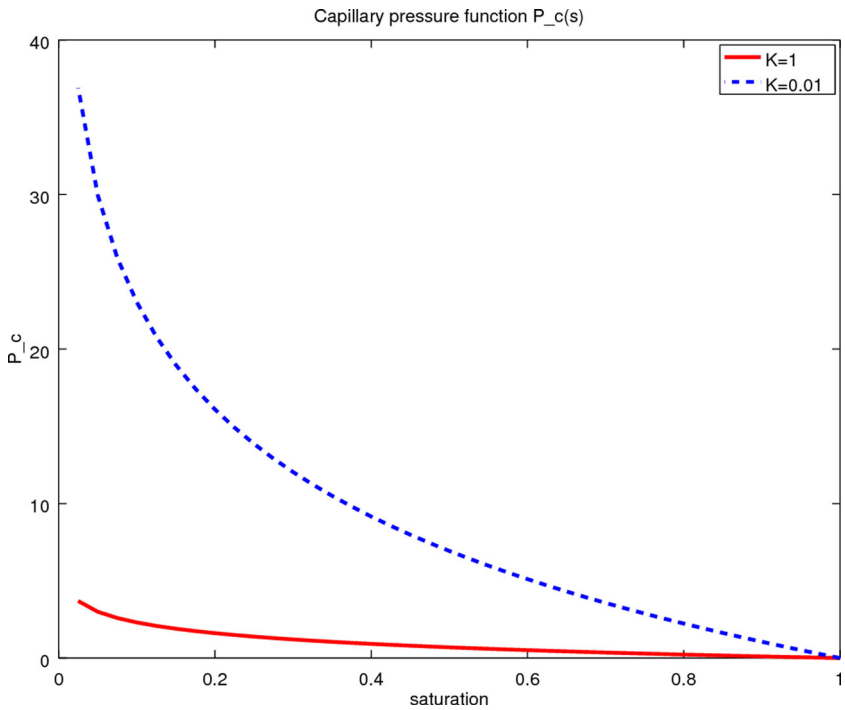

Fig. 2 Capillary pressure function as saturation with different permeability; coefficient $\phi = 1.0$

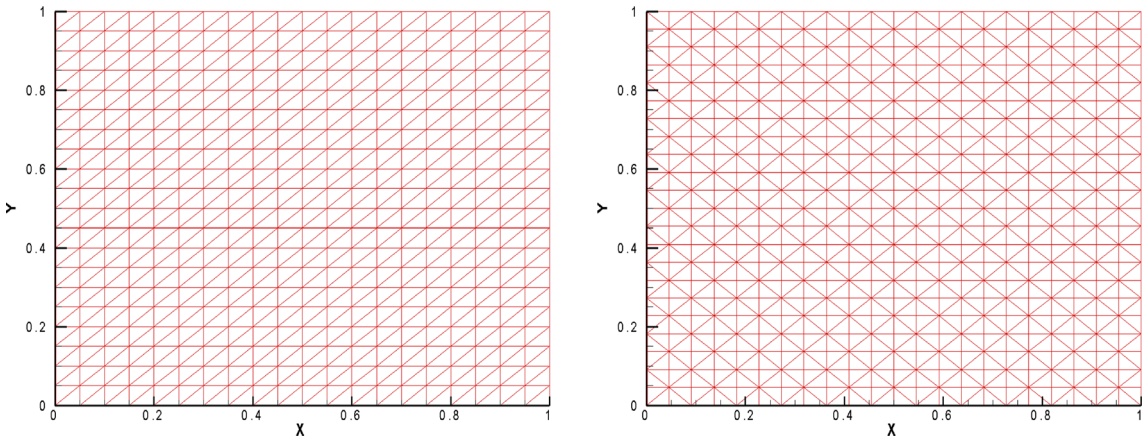

(a) CASE 2: 800 cells (b) CASE 5: 968 cells

Fig. 3 Triangle mesh in Unit domain used by test cases 2 and 5

they are solved sequentially following the IMPES philosophy; First, the pressure equation is solved implicitly, then the saturation equation(s) are solved explicitly. When solving the pressure equation, saturation-dependent quantities such as mobilities and capillary pressure are approximated by values at the old time-level (initial data is used for the first time step). The Generalized Minimum Residual (GMRES) algorithm is used to solve the sparse linear system resulting from the discrete pressure equation and the discrete capillary pressure equation discussed in the next section. The total velocity is calculated after solving the discretised pressure equation and then used in defining the phase continuity equation finite-volume fluxes via the CVD-MPFA formulation. Further details of the discretisation of the saturation equation are given in the next section. We note that by definition, sequential methods cannot satisfy all of the flow equations exactly at each time step of the simulation, e.g. [2].

3 Convective and diffusive flux approximations

3.1 Upwind schemes and entropy satisfaction

The upwind scheme is used with dependence on the direction of the derivative of the convective flux (characteristic speed e.g. [10]). When gravity is included, counter-current flow can occur and requires the use of an entropy satisfying flux. Here, we use the method of [7], where for the *Vt* formulation, the upwind scheme is combined with a Local Lax-Friedrichs(LLF) flux to treat counter-current flow. This is used locally for an entropy fix by the traditional expansion-shock detection method, e.g., the Van Leer Entropy-fix [10], however the wave speed in the LLF scheme is sampled at the Gauss points [7]. In contrast, we have not found any discussion or application in the literature of the *Va* formulation when gravity is present, and the current *Va* formulation lacks an entropy condition. The

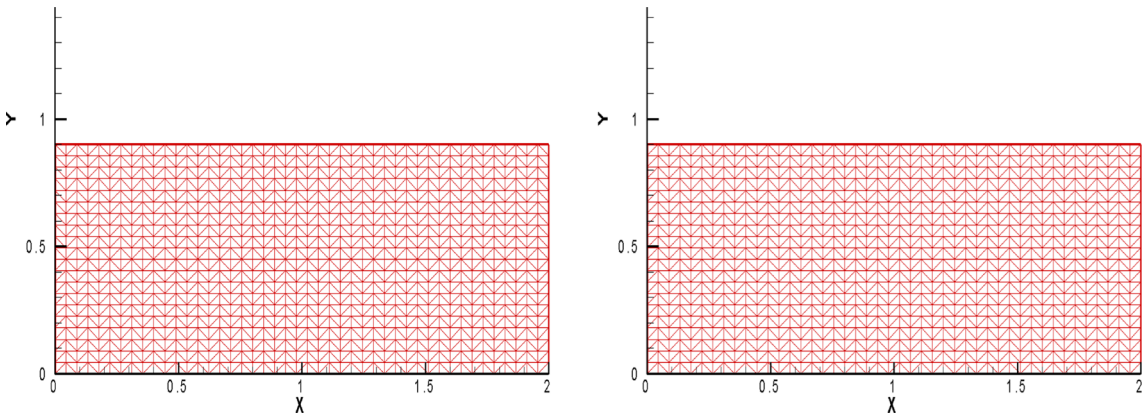

(a) CASE 3 (b) CASE 4

Fig. 4 1800 triangle cells in domain $[0, 2] \times [0, 0.9]$

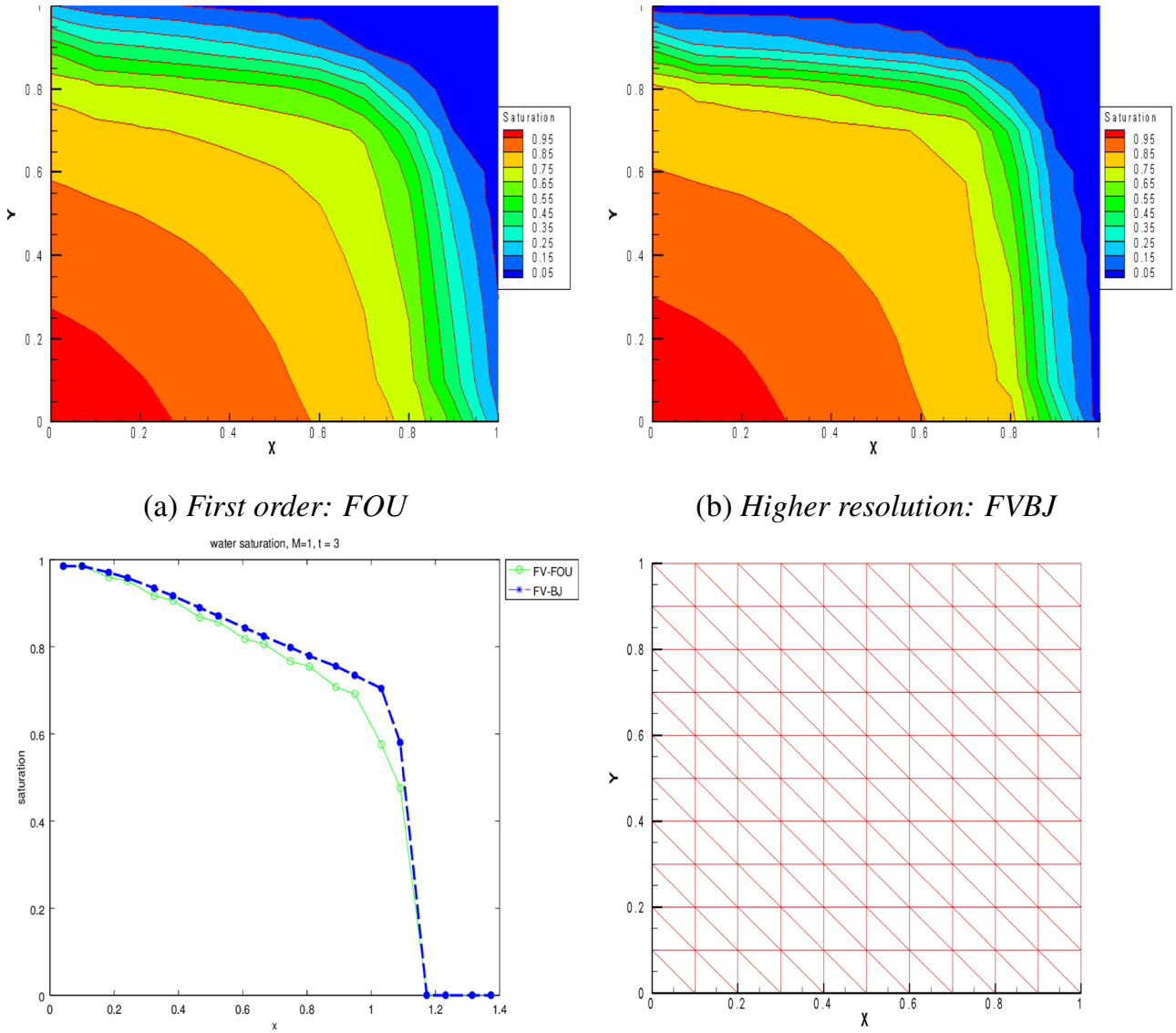

(a) *First order: FOU*

(b) *Higher resolution: FVBJ*

(c) *Cross-section profiles along the domain diagonal*

(d) *grid*

Fig. 5 Isotropic case; $M = 1.0$; $time = 0.5pvi$; 200 triangle cells; Saturation contours

comparison between the *Vt* and *Va* formulations in the presence of gravity with counter current flow is one of the key contributions presented below.

3.2 Higher-resolution reconstructions

Here, we summarize the convective upwind flux approximations and the Barth and Jespersen limiter [1] that is employed in this work. The model equation concerned here is

$$\int_{\Omega} \Phi S_t + div \cdot \vec{\mathsf{F}}\, dV = 0, \tag{16}$$

where $\vec{\mathsf{F}} = f_w(\vec{v}_T + \lambda_o \Delta\rho g \mathbf{K}\nabla h)$ and approximation of the capillary pressure term is discussed in the next sub-section.

We let index i represent the left hand side cell, j represent the right hand side cell and ij the face between i and j cells. The discrete integrated *Vt* numerical flux used in approximating the divergence term of Eq (16) is denoted by $F_{ij}(S_{i,j}, S_{j,i})$ and defined by

$$F_{ij}(S_{i,j}, S_{j,i}) = \frac{1}{2}[(F(S_{j,i}) + F(S_{i,j})) - |\lambda|(S_{j,i} - S_{i,j})] \tag{17}$$

where for the *Vt* formulation $F(S_{i,j})$ and $F(S_{j,i})$ are integrated point values of $\vec{\mathsf{F}}$, and $\lambda = \frac{\Delta F}{\Delta S}$ is computed along the

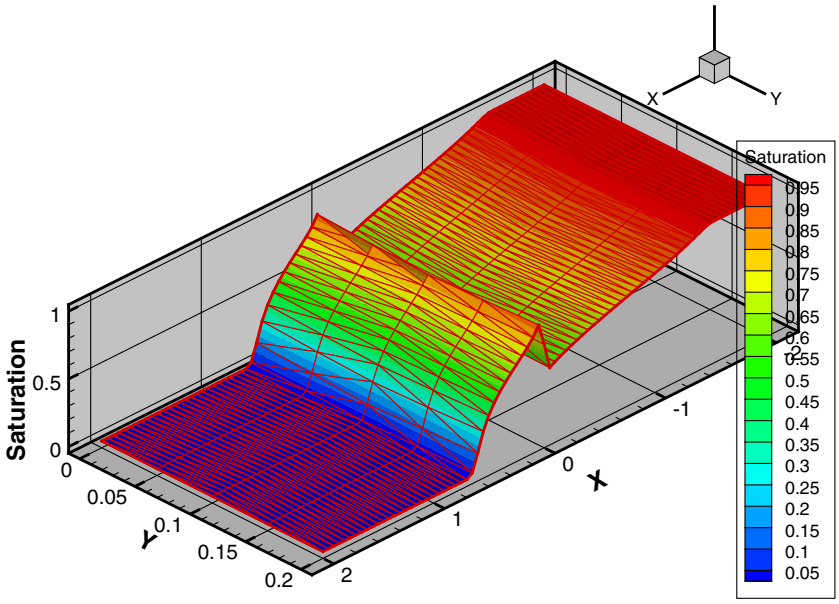

Fig. 6 Implicit CVD-MPFA Tests of two-phase flow on an unstructured mesh; Mesh size: $h_{size} = 0.05$

normal of each face. Note for the first-order upwind method $S_{i,j} = S_i$ and $S_{j,i} = S_j$. If counter current flow is detected then $|\lambda|$ is replaced by $|\lambda_{LLF}|$ following [7]. In contrast the integrated *Va* numerical flux used in approximating the divergence term of Eq (12) depends on upwind data defined according to the sign of $\vec{v}_a$ at each control-volume interface.

In constructing the higher order approximations for both *Vt* and *Va* formulations, we now focus on the data approximations either side of a control-volume face or triangle /quad edge. For the left state of edge ij, the higher order left state saturation is initially unconstrained and defined by $S_{ij} = S_i + L_{ij}(S)$ where $L_{ij} = \Delta x_{ij} \nabla S_i$, Δx_{ij} is the length from cell i's centroid to mid-point of edge ij and the gradient ∇S_i is computed via least squares using the local triangle gradients associated with triangle i. Similarly the higher order right state saturation is initially defined by $S_{ji} = S_j + L_{ji}(S)$ where $L_{ji} = \Delta x_{ji} \nabla S_j$, Δx_{ji} is the length from cell j's centroid to mid-point of edge ij and ∇S_j is the least squares gradient computed with respect to cell j. The limiter proposed by Barth and Jespersen [1] is designed to make sure the reconstructed values satisfy:

A: The reconstruction must not decrease below the minimum or exceed the maximum of the neighbouring cell averages;

B: The difference in the interpolated values at the ij-th edge and the difference in the corresponding cell-averages should have the same sign.

The Barth-Jespersen Limiter is defined by:

$$\Pi_j = \begin{cases} min\left(1.0, \frac{M_i - S_i}{S_{ij} - S_i}\right), & S_{ij} > S_i \\ min\left(1.0, \frac{m_i - S_i}{S_{ij} - S_i}\right), & S_{ij} < S_i \\ 1.0, \ otherwise \end{cases} \tag{18}$$

where

$$m_i = min_{j \in N_i} S_j, M_i = max_{j \in N_i} S_j,$$

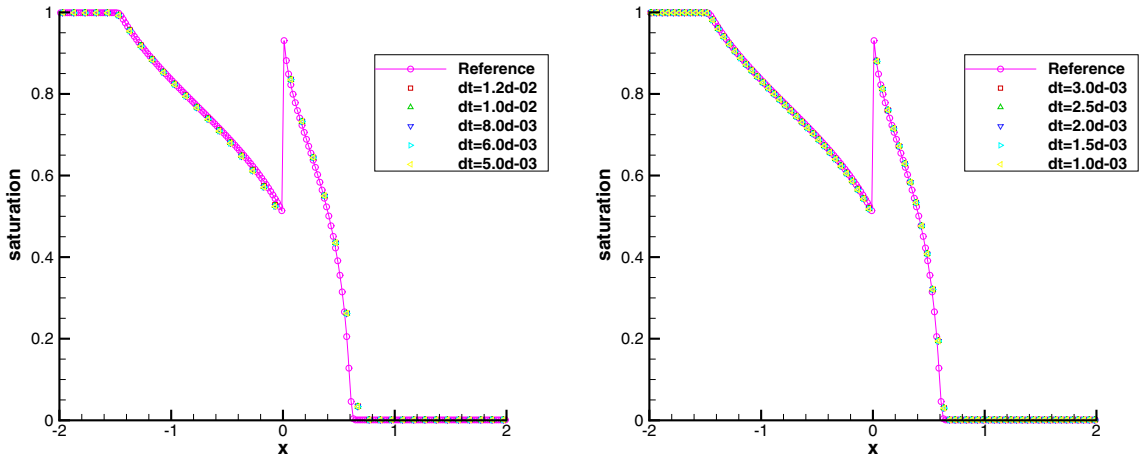

Fig. 7 Implicit CVD-MPFA Tests of two-phase flow on an unstructured mesh; Mesh size *left*: $h_{size} = 0.1$; *right*: $h_{size} = 0.05$

Table 1 Configurations: $h_{size} = 0.1$, $t_{out} = 2.0$

Test index	Δt_{cap}	Max iterations	*Diff-Num*
Test 1	$1.2 \cdot 10^{-2}$	2	0.920
Test 2	$1 \cdot 10^{-2}$	2	0.767
Test 3	$8 \cdot 10^{-3}$	2	0.613
Test 4	$6 \cdot 10^{-3}$	2	0.460
Test 5	$5 \cdot 10^{-3}$	2	0.383

N_i is the set of direct neighbours of cell i, and $\Pi_i = min_{j \in N_i}[\Pi_j]$.

The local formulation for the reconstruction with respect to edge ij then uses the respective slope limiters to define the higher order left and right hand state saturations:

$$\begin{aligned} S_{ij} &= S_i + \Pi_i L_{ij}(S) \\ S_{ji} &= S_j + \Pi_j L_{ji}(S) \end{aligned} \tag{19}$$

and the flux is a function of the left and the right hand states, c.f. Eq (17), with upwind direction chosen according to the sign of the local wave speed normal to edge ij. The stencil for reconstruction and limiter is depicted in Fig. 1.

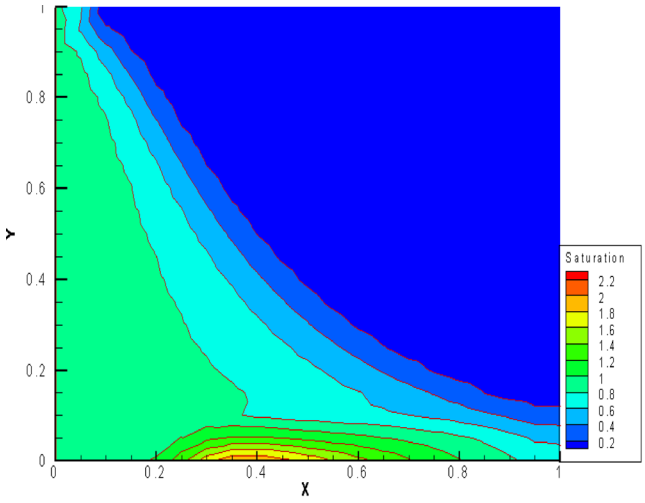

(a) *Va*; Saturation contours

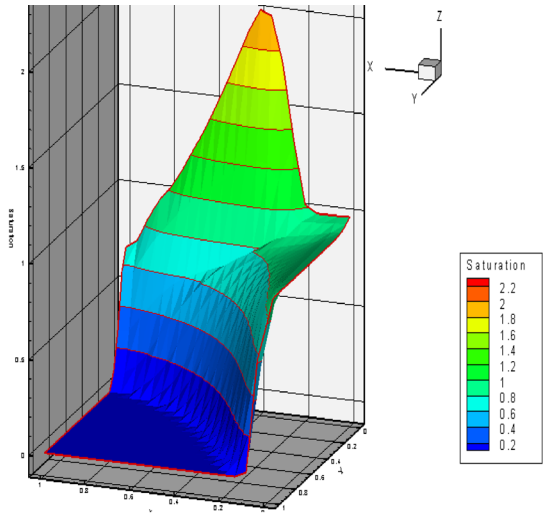

(b) *Va*; Saturation Isosurface

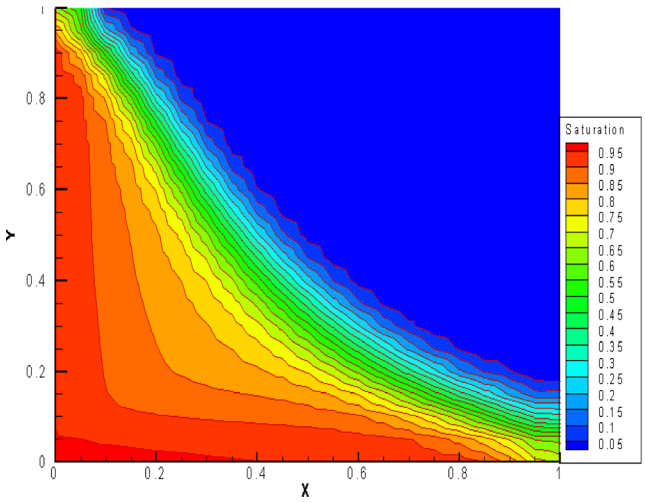

(c) *Vt*; Saturation contours

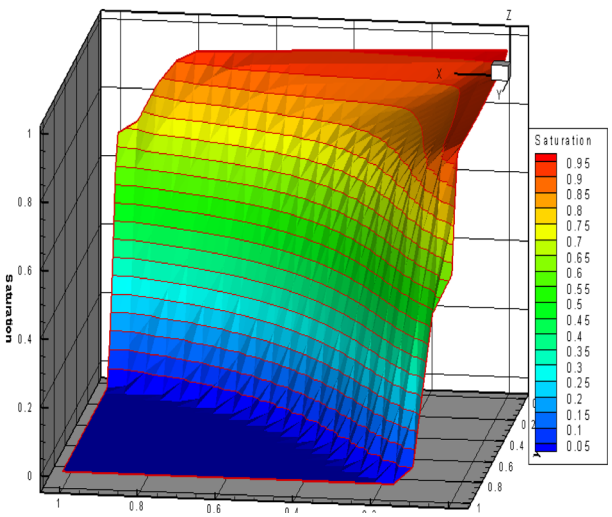

(d) *Vt*; Saturation Isosurface

Fig. 8 CASE 2: $M = 1.0$; $time = 0.5$; 800 triangle cells; FOU

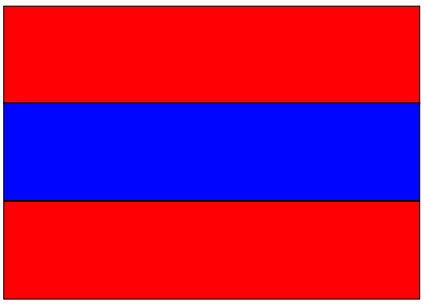

Fig. 9 The domain tested,The middle layer in the domain is least permeable

3.3 Semi-implicit CVD-MPFA method for the unsteady capillary pressure equation

In the *Vt* formulation, an explicit capillary flux approximation adds further restriction to the CFL condition for the saturation equation. In the formulation presented a Godunov time-splitting based strategy is adopted, with an explicit convective update followed by an implicit diffusive (capillary pressure) update. The convective flux is approximated using the above methods of Sections 3.1 and 3.2. Here, we now focus on the diffusive flux. In the explicit case a severe diffusivity time-step limit is imposed as a result of the unsteady capillary pressure flux. To overcome the explicit diffusivity limit an implicit method is used. In this formulation, the CVD-MPFA method is used to approximate the capillary pressure operator, with capillary pressure p_c and capillary flux assumed to be continuous across medium interfaces. When treating the diffusive capillary update, the nonlinear capillary pressure function $p_c = \Psi(s)$, is rearranged and saturation is formally expressed as $s = \Psi^{-1}(p_c)$, which is assumed to be unique, and now the unknown p_c is determined in this step. The equation splitting is expressed in semi-discrete form with respect to time as follows:

$$\Phi \frac{(s^* - s^n)}{\Delta t} + \nabla \cdot (f_w(s^n)\vec{v}_T) = q_w, \tag{20}$$

$$\Phi \frac{(s^{n+1} - s^*)}{\Delta t} + \nabla \cdot \left((f_w \lambda_o)(s^{n+1}) \mathbf{K} \nabla {p_c}^{n+1} \right) = 0. \tag{21}$$

For an implicit formulation equation (21) is rewritten in terms of p_c as

$$\Phi \frac{\Psi^{-1}(p_c^{n+1}) - \Psi^{-1}(p_c^*)}{\Delta t} + \nabla \cdot \left(f_w \lambda_o (\Psi^{-1}(p_c^{n+1})) \mathbf{K} \nabla p_c^{n+1} \right) = 0, \tag{22}$$

For an implicit method using Backward-Euler, two time discretization variants have been considered for approximation of the non-linear terms, (i) Newton-Raphson Iteration and (ii) a Predictor-Corrector linearisation: We found the latter to be far more efficient and it is expanded below.

Predictor-corrector fixed-point iteration method An iterative linearisation is presented, which does not explicitly depend on $\Psi^{-1}(p_c)$. The linearisation employs the derivative approximation (see Peaceman [12]) where

$$s^{n,i+1} = s^{n,i} + \frac{ds}{dp_c}(p_c^{n,i})(p_c^{n,i+1} - p_c^{n,i}). \tag{23}$$

to form an iterative method to solve Eq. 22 written as

$$\frac{\Phi|\Omega|}{\Delta t} \left(s^{n,i} + \frac{ds}{dp_c}(p_c^{n,i})(p_c^{n,i+1} - p_c^{n,i}) - s^{n,0} \right) + \int_{\partial\Omega} (f_w \lambda_o)(s^{n,i}) \mathbf{K} \nabla p_c^{n,i+1} \cdot \vec{n}\, dA = 0, \tag{24}$$

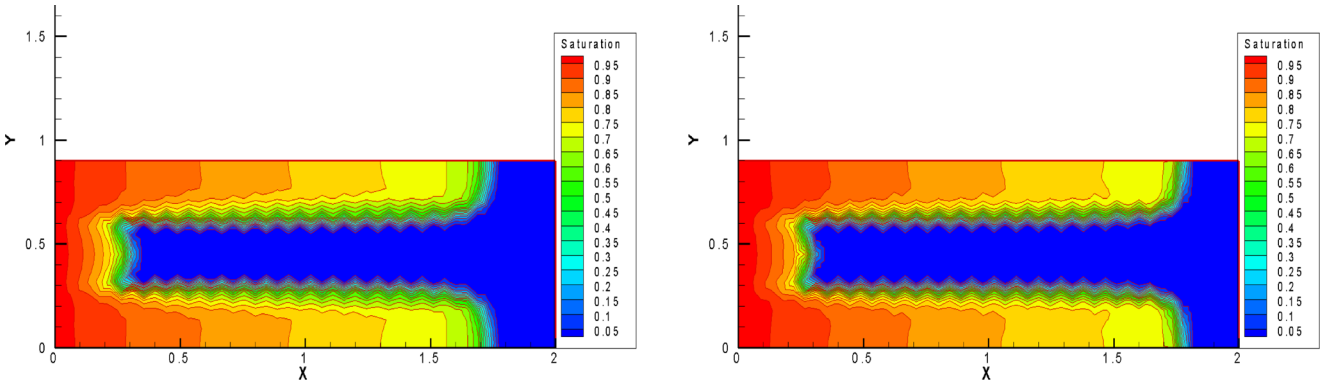

(a) FOU (b) FVBJ

Fig. 10 Saturation contours; $M = 1.0$; $time = 1.0$; *no-capillary pressure*; on triangle mesh; 1800 cells

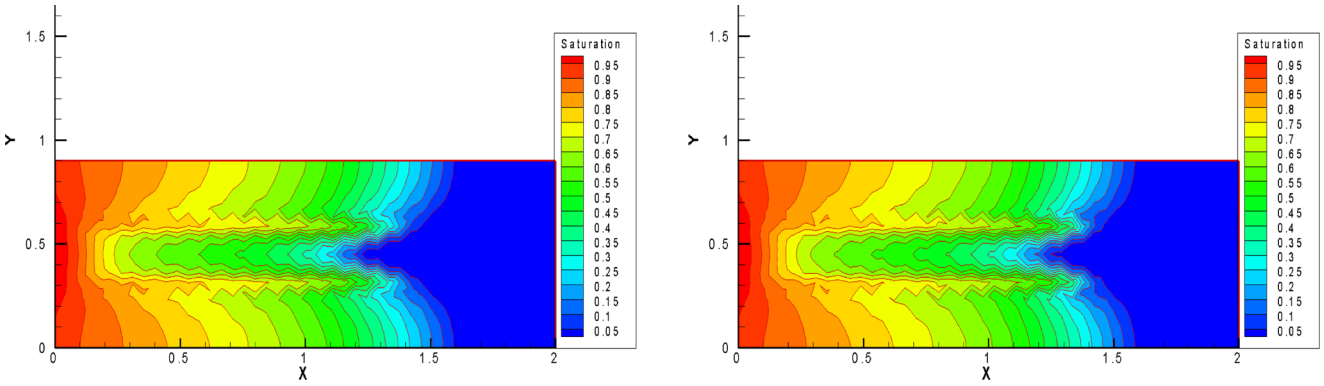

(a) *Va* Explicit (b) *Vt* splitting Semi-Implicit

Fig. 11 Saturation contours; $M = 1.0$; capillary pressure coefficient $\phi = 1.0$; $time = 1.0$; FVBJ; on triangle mesh; 1800 cells

and rearranged in the form

$$\boxed{\frac{\Phi|\Omega|}{\Delta t}\frac{ds}{dp_c}(p_c^{n,i})}p_c^{n,i+1}+\int_{\partial\Omega}\boxed{(f_w\lambda_o)(s^{n,i})}\mathbf{K}\nabla p_c^{n,i+1}\cdot\vec{n}\,dA$$
$$=\boxed{\frac{\Phi|\Omega|}{\Delta t}\left(\frac{ds}{dp_c}(p_c^{n,i})p_c^{n,i}+s^{n,0}-s^{n,i}\right)}. \quad (25)$$

where in the above equations the boxed coefficients are approximations that converge as the iteration converges with $(p_c^{n,i+1} - p_c^{n,i}) \Longrightarrow 0$. The initial iteration condition is $p_c^{n,0} = p_c^*, s^{n,0} = s^*$.

The algorithm is described below:

Step 1: $s^{n,i} = s^*$, $p_c^{n,i} = p_c^*$.

Step 2: solve the global equations (25) through the domain.

Step 3:

$s^{n+1} = s^{n,i+1}$, if $max\left(\frac{abs(s^{n,i+1}-s^{n,i})}{s^{n,i}}\right) < TOL$;

$s^{n,i} = s^{n,i+1}$, $p_c^{n,i} = p_c^{n,i+1}$ then repeat from Step 2, otherwise.

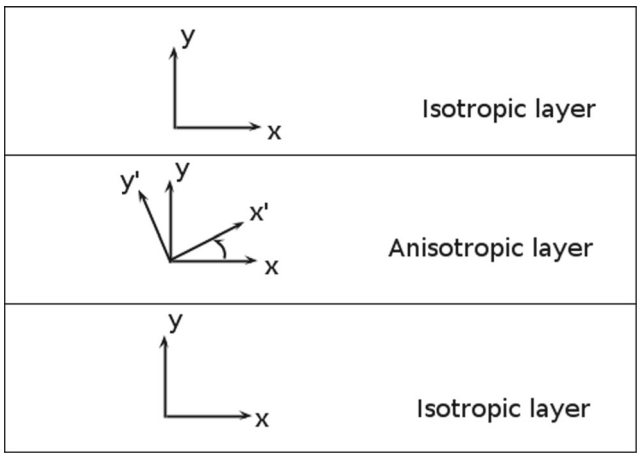

Fig. 12 Domain with a full permeability tensor in the middle layer

We note that [14] employed a similar linearisation with constant derivative in the iteration applied to a global pressure formulation and convergence of the iterative process was shown. We now consider a variety of tests on structured and unstructured grids.

4 Results

The first test case demonstrates the effectiveness of the higher resolution method. The second case demonstrates the effectiveness of the linearisation. The other cases that follow contrast the performance of *Vt* versus *Va* for convective flow, and convective flow with gravity and capillary pressure. In these test cases, the capillary pressure function is defined as

$$\Psi(s) = -\frac{\phi}{\sqrt{k}}ln(s), \quad (26)$$

and the inverse function is $s = \Psi^{-1}(p_c) = e^{-\frac{\sqrt{k}}{\phi}p_c} \cong 1 - \frac{\sqrt{k}}{\phi}p_c$, where ϕ is a specified constant in the tests. Example curves are shown in Fig. 2 in this work we assume $\lambda_o = (1-s)^m$, $\lambda_w = s^m$, where $m = 2$.

The first-order upwind method is denoted by FOU while the higher resolution finite-volume Barth-Jesperson method is denoted by FVBJ. The meshes used in the following tests are shown in Figs. 3 and 4. Unless stated otherwise, for all test cases the initial water saturation is 0.0001 throughout the field, at inflow saturation is unity and reflection conditions apply on solid walls. Here $\rho_w = 1$ and $\rho_o = 0.8$.

4.0.1 CASE 0: quarter-five spot

We begin with a comparison of results obtained using the respective first order upwind and the higher resolution

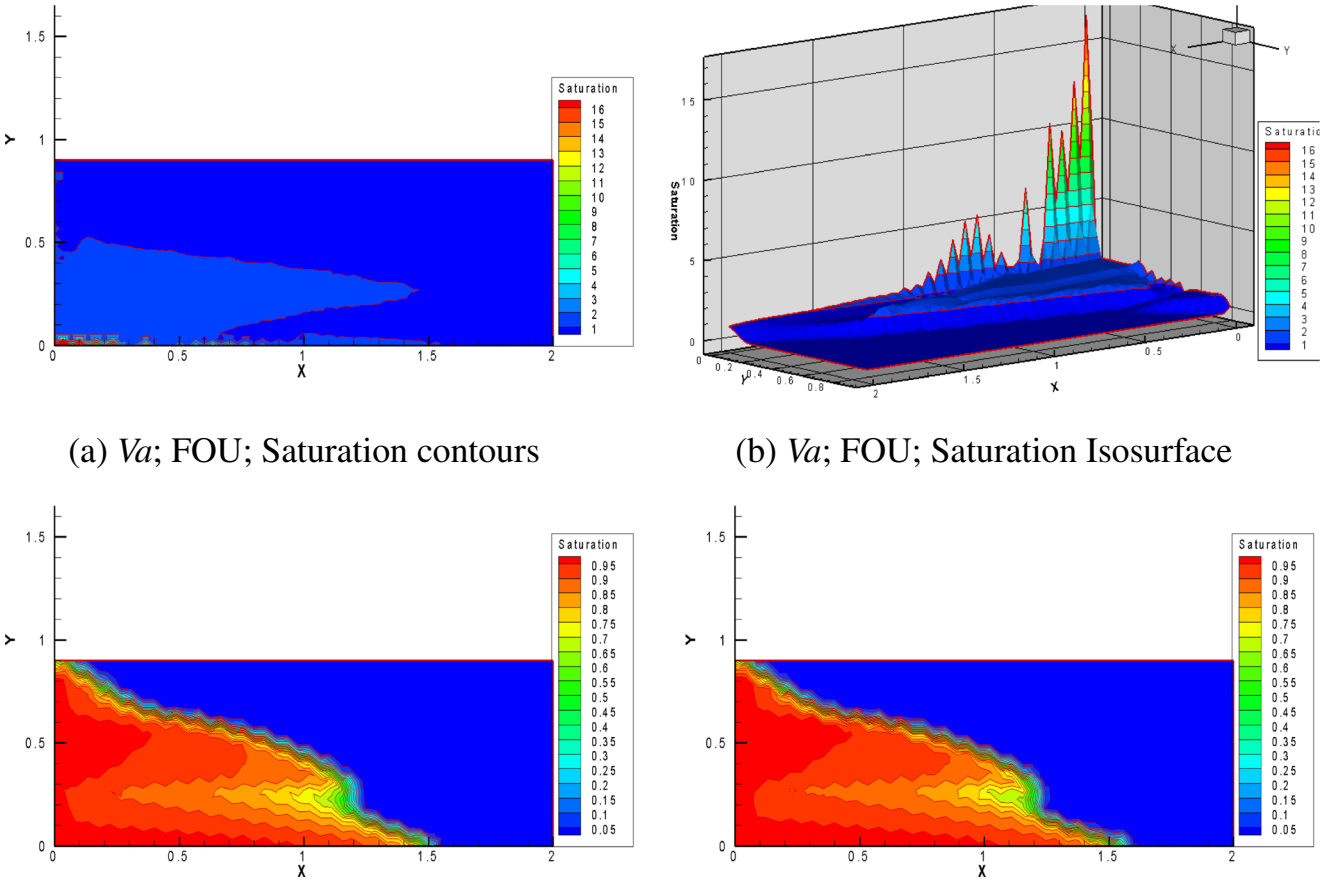

(a) *Va*; FOU; Saturation contours

(b) *Va*; FOU; Saturation Isosurface

(c) *Vt*; FOU; Saturation contours

(d) *Vt*; FVBJ; Saturation contours

Fig. 13 $M = 1.0$; $time = 0.8$; capillary pressure coefficient $\phi = 0.0$; on triangle mesh; 1800 cells

methods applied to the classical quarter-five spot problem, with the initial condition of saturation is$S_0(\vec{x}) = S_{wc} = 0.0001, \vec{x} \in [0, 1] \times [0, 1]$. An isotropic rock permeability matrix is considered with $K_m = I$. The problem involves an injection well(bottom left), with specified flow rate $q = 0.1$, a production well (top right) where pressure is specified, and solid wall conditions imposed on all boundaries. The results of this non-linear case are shown at $0.5pvi$ in Fig. 5. We note that since capillary pressure and gravity are absent, then in this case the *Vt* and *Va* formulations are identical.

4.0.2 CASE 1: 1D capillary pressure convergence tests

This case involves a demonstration of the performance of the implicit capillary pressure linearisation (used in the *Vt* formulation) on a well established one dimensional problem [3, 8], that is driven by capillary pressure effects governed by Eq. 22. The domain is a rectangle $(x, y) \in [-2, 2] \times [0, 0.2]$, and an unstructured mesh is used. The permeability field is given by:

$$k(x) = \begin{cases} 4.2025, x < 0.0 \\ 0.5625, x > 0.0 \end{cases} \tag{27}$$

The initial conditions for saturation are

$$S_0(x) = \begin{cases} 0.999, x < 0.0 \\ 0.001, x > 0.0 \end{cases} \tag{28}$$

water and oil viscosity are set to be $\nu_w = 1.0$, $\nu_o = 1.0$. For simplicity, the porosity of the medium is set to be $\Phi = 1.0$, and $s_{wc} = s_{or} = 0.0$. The capillary pressure via the inverse function of $s = \psi(p_c)$ is used as the unknown, and the above linearisation is adopted, Results are computed at $t = 2.0$.

The results are shown at sample position $y = 0.1$, and are presented in Figs. 6 and 7. Table 1 demonstrates the efficiency of the iteration method.

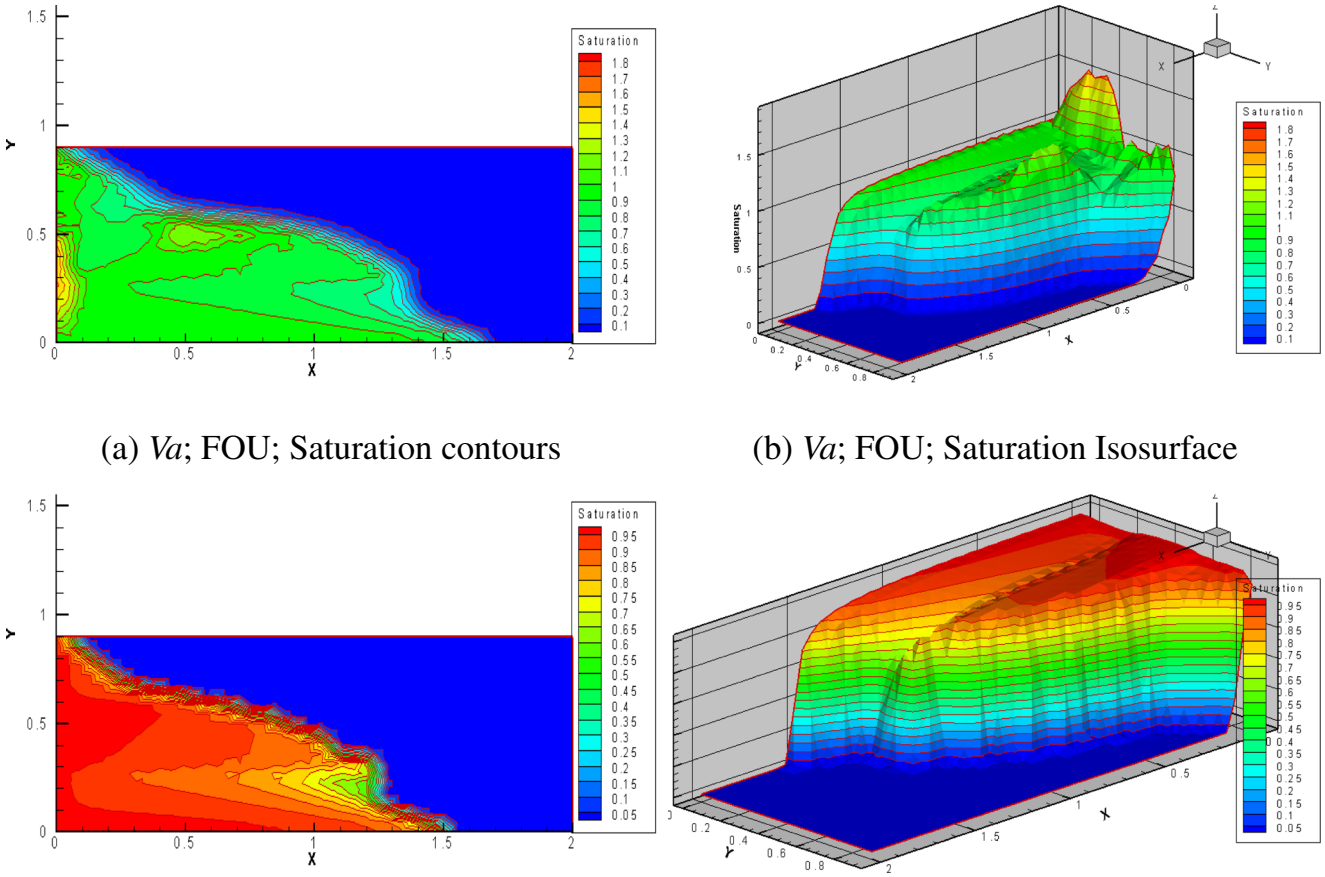

(a) *Va*; FOU; Saturation contours

(b) *Va*; FOU; Saturation Isosurface

(c) *Vt*; FOU; Saturation contours

(d) *Vt*; FOU; Saturation Isosurface

Fig. 14 $M = 1.0$; $time = 0.8$; capillary pressure coefficient $\phi = 0.05$; on triangle mesh; 1800 cells

The *diffusivity number* on a 2D triangle mesh is defined by:

$$Diff\text{-}Num = max_{i\in[1,N]} \left\{ \frac{\Delta t}{vol_i} max_{j\in[1,3]} \left\{ K_i \frac{\partial (f_w \lambda_o \nabla p_c)(s_i)}{\partial s} \cdot \vec{n}_j \right\} \right\}, \quad (29)$$

where N is the total number of cells in the domain, vol_i is the cell volume, and $\vec{n}_j$ is the outward normal of the j-th edge, scaled by the edge length. As noted in, e.g., [19], the stability condition $Diff\text{-}Num \leq \frac{1}{3}$ must be satisfied when an explicit scheme is used (on a 2D cartesian grid this would be $\frac{1}{4}$). Here this condition is removed by using the implicit scheme.

4.1 Comparisons between *Vt* and *Va* Formulations

CASE 2: channel flow with gravity Water is injected at the left-hand side boundary where a Neumann condition is imposed with flux $f_l = 1.0$. A Dirichlet condition is specified on the right boundary, $p_r = 1.0$. Solid wall conditions apply on upper and lower boundaries. Gravity acts in the vertical direction. The permeability tensor is isotropic with a unit diagonal tensor. The results from using the respective *Va* and *Vt* formulations are shown in Fig. 8. The results in Fig. 8a, b show that the *Va* formulation is unable to resolve counter-current flow, with incorrect upwinding causing a build up of water saturation adjacent to the solid wall. In contrast the *Vt* formulation with entropy fix is able to resolve the interaction of convective and gravity forces, as shown in the results in Fig. 8c, d.

CASE 3: layered channel flow We consider displacement of oil by water in a 3 layered rectangular domain, initially filled with oil, which is shown in Fig. 9. The permeability is isotropic with value 0.01 in the middle layer and 1 otherwise. Water is injected uniformly at the left hand boundary. The boundary conditions involve a Neumann flux $f_l = 1.0$ on the left hand boundary, and a Dirichlet condition, $p_r = 1.0$ on the right hand boundary. Solid wall conditions apply on upper and lower boundaries.

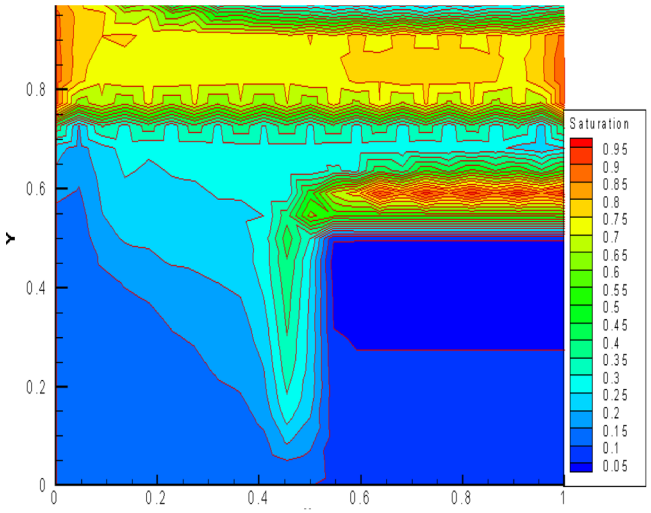

(a) No capillary, no entropy-fix

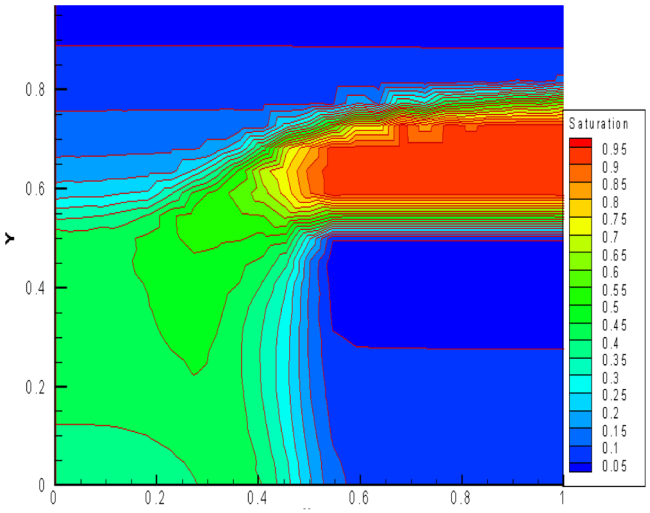

(b) No capillary, entropy-fix

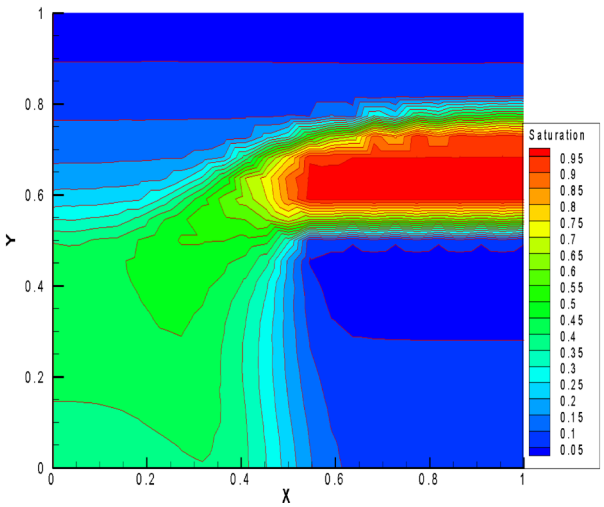

(c) explicit capillary, $\phi = 0.01$, entropy-fix

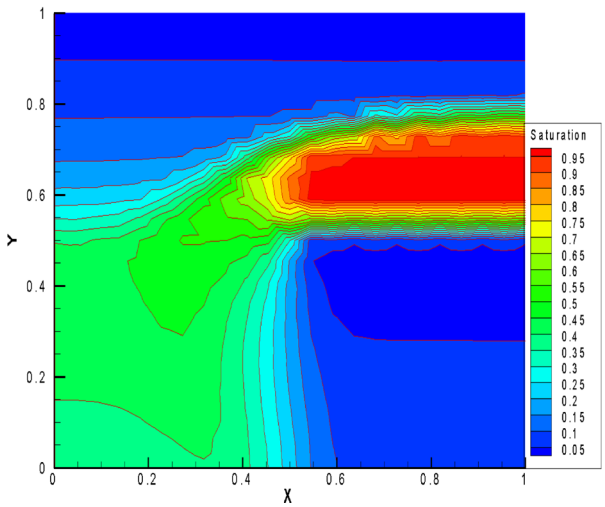

(d) implicit capillary, $\phi = 0.01$, entropy-fix

Fig. 15 Saturation contours; *Vt*; $M = 1.0$; $time = 1.25$; FOU; 968 triangle cells

The results for convective two-phase flow without gravity or capillary pressure are shown in Fig. 10 and demonstrate the benefit of the higher resolution method. Two-phase flow results with capillary pressure (zero gravity) are shown in Fig. 11, this case compares with [8]. In this case, *Va* and *Vt* yield similar results. The effect of capillary pressure is seen by contrasting Fig. 11 with Fig. 10.

CASE 4: layered channel flow with gravity and a discontinuous full permeability tensor The domain is comprised of three horizontal layers, shown in Fig. 12. The upper and lower layers have unit isotropic permeability, while the central layer has a full permeability tensor with principal values $(K_1, K_2) = (10, 1)$ rotated at an angle θ of 30 degrees to the horizontal. The permeability tensor is defined by

$$\vec{K} = \begin{bmatrix} cos\theta & -sin\theta \\ sin\theta & cos\theta \end{bmatrix} \begin{bmatrix} K_1 & 0 \\ 0 & K_2 \end{bmatrix} \begin{bmatrix} cos\theta & sin\theta \\ -sin\theta & cos\theta \end{bmatrix} \tag{30}$$

Gravity acts vertically and capillary pressure is included and tested, results for coefficient strengths $\phi = 0.0, 0.05$ are shown, respectively. Water is injected at the left-hand-side

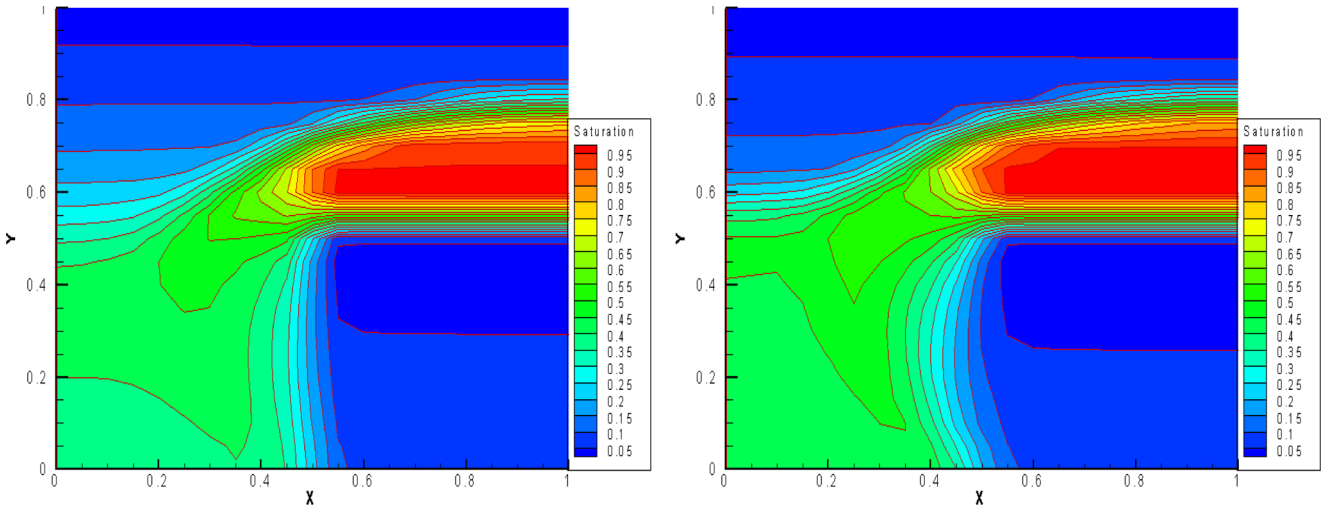

(a) FOU; 20x20 quad cells

(b) FVBJ; 20x20 quad cells

(c) FOU; 64x64 quad cells

(d) FVBJ; 64x64 quad cells

Fig. 16 *Vt* Saturation contours, Low order versus Higher order FVBJ; $M = 1.0$; zero capillary pressure $\phi = 0.0$; $time = 1.25$

boundary, with boundary conditions as follows: Left boundary, Neumann flux $f_l = 1.0$. On the right-hand boundary, the Dirichlet condition $p_r = 1.0$ is imposed. Solid wall conditions are applied on the top and bottom boundaries. The *Va* formulation results in Figs. 13a, b and 14a, b show that the *Va* formulation is unstable without capillary pressure $\phi = 0.0$ and with capillary pressure $\phi = 0.05$. In contrast, the *Vt* formulation results of Fig. 13c, d (which also shows the higher resolution result) and Fig. 14c, d show that the *Vt* formulation is stable and resolves the resulting flow for both cases.

CASE 5: shale barrier with gravity driven flow This case is purely gravity driven and defined over a square domain of unit length $[0, 1]X[0, 1]$. Water is initially on top of oil forming two fluid layers with an interface at $y = 0.75$ above a solid shale barrier defined at $y = 0.5$, for $[0.5 \leq x \leq 1]$.

$$s_w = \begin{cases} 1.0, \; y > 0.75 \\ 0.1, \; otherwise \end{cases} \tag{31}$$

The permeability is isotropic and set to unity. A Dirichlet condition for pressure is specified at the lower boundary with $p_b = 1.0$. Solid wall conditions are imposed at other boundaries.

The necessity of the entropy fix used for the *Vt* formulation is illustrated by comparing the results of Fig. 15a, b, where Fig. 15a is computed without an entropy fix and

Fig. 15b is computed with the entropy fix. The effect of the saturation dependent capillary-pressure flux time level on the *Vt* formulation results is illustrated in Fig. 15c, d, where the result of Fig. 15c is computed with an explicit capillary pressure flux, while that of Fig. 15d is computed with an implicit flux. All other *Vt* formulation results in this paper involving capillary-pressure are computed with an implicit capillary-pressure flux.

The benefit of the higher resolution *Vt* formulation versus the first order *Vt* formulation (with zero capillary pressure) is shown in Fig. 16 where improved resolution of the saturation field is obtained by the FVBJ method. The results of Fig. 17 show *Va* Fig. 17a, b versus *Vt* Fig. 17c, d when capillary pressure (small coefficient $\phi = 0.01$) is added. The *Va* results of Fig. 17a, b show that for small (or zero) capillary pressure, the *Va* method which lacks an entropy condition cannot resolve counter-current flow. Comparing the *Vt* results of Figs. 16a and 17c shows that the added capillary pressure still has a significant effect on results, where the shock front is seen to start spreading in (Fig. 17c) due to the diffusive capillary effect. The *Va* method begins to resolve the flow for higher capillary pressure ($\phi = 0.05$) as shown in the comparison between *Va* and *Vt* in Fig. 18. However, even at higher capillary pressure, the *Va* results indicate some instability c.f. Fig. 18b compared to *Vt* Fig. 18d.

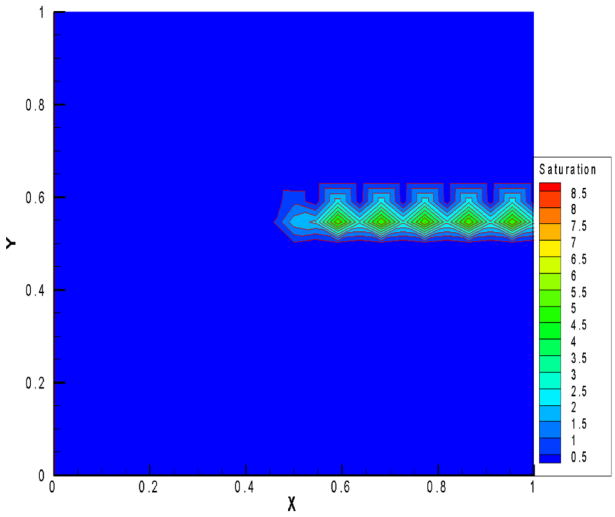

(a) *Va*; Saturation contours

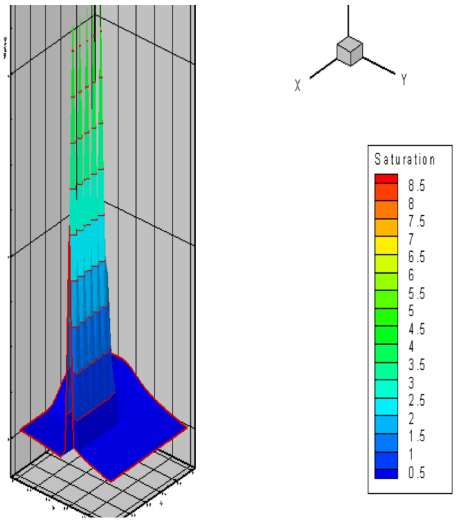

(b) *Va*; Saturation Isosurface

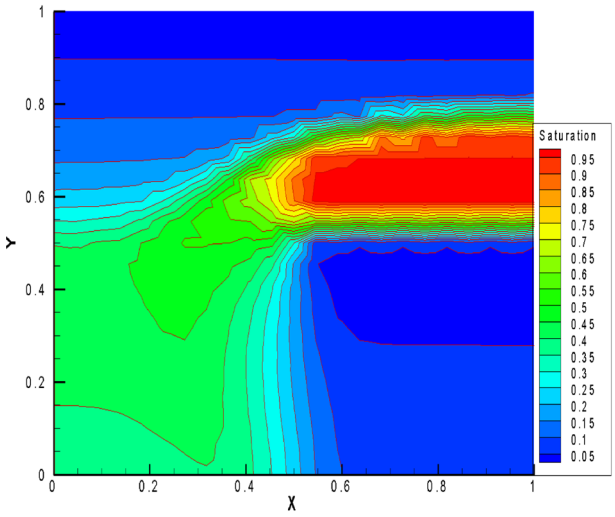

(c) *Vt*; Saturation contours

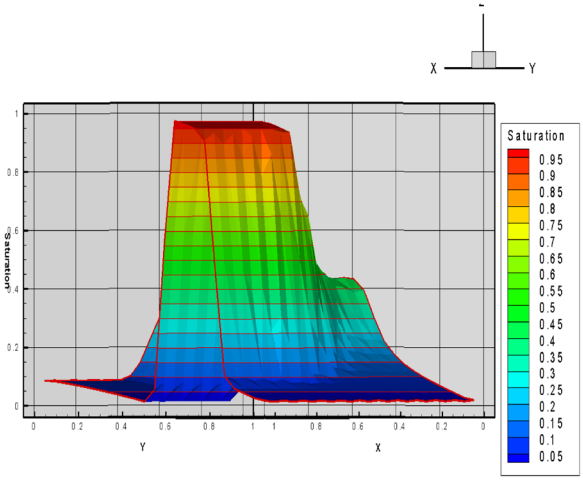

(d) *Vt*; Saturation Isosurface

Fig. 17 $M = 1.0$; capillary pressure coefficient $\phi = 0.01$; $time = 1.25$; FOU; 968 triangle cells

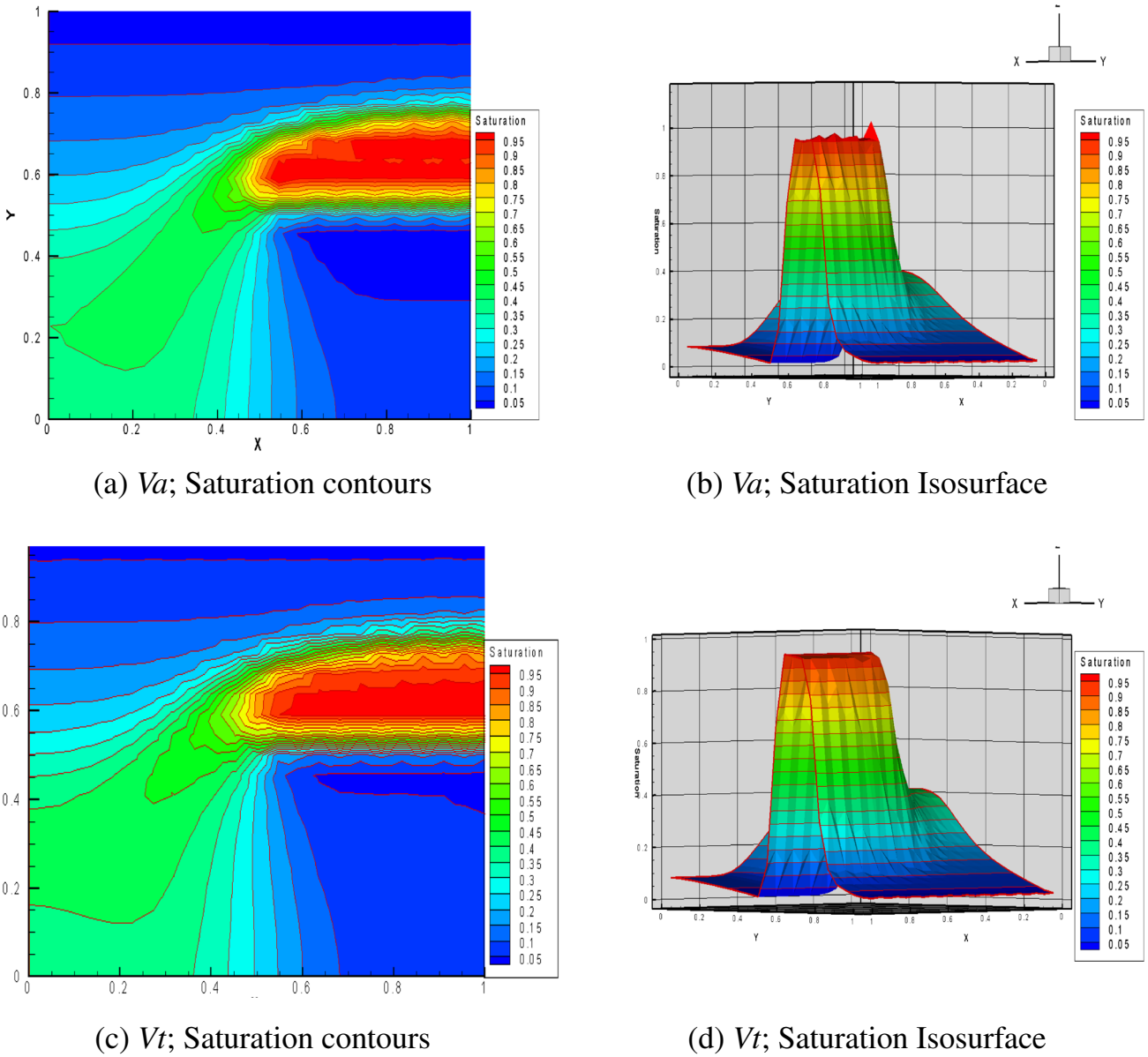

(a) *Va*; Saturation contours

(b) *Va*; Saturation Isosurface

(c) *Vt*; Saturation contours

(d) *Vt*; Saturation Isosurface

Fig. 18 $M = 1.0$; capillary pressure coefficient $\phi = 0.05$; $time = 1.25$; FOU; 968 triangle cells

5 Conclusions

An unstructured cell-centred higher resolution finite-volume framework for porous media flow simulation is presented. Two formulations *Vt* and *Va*, are presented and contrasted for simulation of two-phase flow including gravity and capillary pressure. The implicit linearisation proves effective for the capillary pressure term. The CVD-MPFA method is used for Darcy-flux approximation including pressure, gravity and capillary-pressure flux components. Test cases are presented for comparison of the two formulations. The *Vt* formulation proves to be robust for all cases tested. When computing solutions involving gravity with counter-current flow, the *Va* formulation, which lacks an entropy condition, yields unstable results. For problems with smaller gravity to capillary force ratios and consequently less dependence on an imposed entropy condition, stability of the *Va* formulation may improve. However, the results presented show that the *Va* formulation can prove to be unstable when gravity is present in the flow problem. The benefit of the higher resolution *Vt* method compared to the first order method is also demonstrated.

Acknowledgements We thank Dr's S. Lamine and B. Huisman of Shell and M. Pal of Maersk for helpful discussions.

References

1. Barth, T., Jespersen, D.C.: The design and application of upwind schemes on unstructured meshes. AIAA paper 89–0366 (1989)
2. Trangenstein, J.A.: Multi-phase Flow in Porous Media: Mechanics, Mathematics and Numerics. Lecture Notes, IBM Scientific Center, Bergen, Norway. UCLR-97053 Lawrence Livermore National Laboratory, USA (1987)
3. van Duijn, C.J., de Neef, M.J.: Similarity solution for capillary redistribution of two phases in a porous medium with a single discontinuity. Adv. Water Resour. **21**, 451–461 (1998)
4. Karimi-Fard, M., Firoozabadi, A.: Numerical simulaton of water injection in 2-D fractured media using discrete fractured model. SPE RE & E, 117–126 (2003)
5. Edwards, M.G.: Higher-resolution hyperbolic-coupled-elliptic flux-continuous CVD schemes on structured and unstructured grids in 2-D. Int. J. Numer. Methods Fluids **51**, 1059–1077 (2006)
6. Friis, H.A., Edwards, M.G., Mykkeltveit, J.: Symmetric positive definite flux-continuous full-tensor finite-volume schemes on unstructured cell centered triangular grids. SIAM J. Sci. Comput. **31**(2), 1192–1220 (2008). https://doi.org/10.1137/070692182
7. Edwards, M.G.: Global and local central non-upwind finite volume schemes for hyperbolic conservation laws in porous media. Int. J. Numer. Meth. Fluids **64**(7), 793–811 (2010)
8. Friis, H.A., Evje, S.: Numerical treatment of two-phase flow in capillary heterogeneous porous media by finite-volume approximations. Int. J. Numer. Anal. Mod. **9**(3), 505–528 (2012)
9. Hoteit, H., Firoozabadi, A.: Numerical modeling of two-phase flow in heterogeneous permeable media with different capillarity pressures. Adv. Water Resour. **31**, 56–73 (2008)
10. Leveque, R.J.: Finite-Volume Methods for Hyperbolic Problems. Cambridge University Press (2004)
11. Godunov, S.K.: A finite difference method for the numerical computation of discontinuous solutions of the equations of fluid dynamics, Mat. Sb. (1959)
12. Peaceman, D.W.: Fundamentals of Numerical Reservoir Simulation. Elsevier, Amsterdam/New York (1977)
13. Aziz, K., Settari, A.: Petroleum Reservoir Simulation. Elsevier (1979)
14. Radu, F.A., Nordbotten, J.M., Pop, I.S., Kumar, K.: A robust linearization scheme for finite volume based discretizations for simulation of two-phase flow in porous media. J. Comput. Appl. Math. https://doi.org/10.1016/j.cam.2015.02.051 (2015)
15. Bastian, P.: A fully-coupled discontinuous galerkin method for two-phase flow in porous media with discontinuous capillary pressure. arXiv:1309.7555v1 (2013)
16. Brenier, Y., Jaffre, J.: Upstream differencing for multiphase flow in resorvoir simulation. SIAM J. Numer. Anal. **28**(3), 685–696 (1991). https://doi.org/10.1137/0728036
17. Kaasschieter, E.: Solving the buckley-leverett equation with gravity in a heterogeneous porous medium. Comput. Geosci. **3**(1), 23–48 (1999). https://doi.org/10.1023/A:1011574824970
18. Wheeler, M.F., Xue, G.: Accurate locally conservative discretizations for modeling multiphase flow in porous media on general hexahedra grids. ECMOR XII (2010)
19. Batten, P., Lambert, C., Causon, D.M.: Positively conservative high-resolution convection schemes for unstructured elements. Int. J. Numer. Methods Eng. **39**(11), 1821–1838 (1996)